Phase formation induced by ion irradiation and electrical resistivity of aluminum–3*d*-transition-metal alloys

N. Karpe,* K. Kyllesbech Larsen, and J. Bøttiger
Institute of Physics and Astronomy, University of Aarhus, DK-8000, Aarhus C, Denmark
(Received 21 January 1992)

The phase formation, in particular amorphization, caused by 500-keV Xe^+ ion irradiation of thin multilayered films of Al-Ti, Al-V, Al-Cr, Al-Mn, Al-Fe, Al-Co, and Al-Ni has been investigated. At a substrate temperature of 100 K during the irradiation, all these alloy systems are found to become amorphous for aluminum-rich compositions. At room temperature, the formation of structurally simple-crystalline solid solutions over extended compositional ranges, as compared to thermodynamic equilibrium, is observed. The electrical resistivity of amorphous $Al_{83}M_{17}$ alloys, where M = Ti, V, Cr, Mn, Fe, Co, or Ni, is found to vary systematically as a function of transition-metal element. A maximum is observed around Fe, for which the *d*-electron states coincide with the Fermi level. This behavior suggests that scattering of the conduction electrons by the 3*d*-electron states plays a dominant role. A comparison with x-ray photoelectron spectroscopy data from the literature suggests that the resistivity of amorphous $Al_{83}M_{17}$ alloys can be directly correlated to the position and width of the *d*-electron states.

I. INTRODUCTION

Thin-film techniques, including ion irradiation of elemental multilayers, have in the recent decade been used successfully to form metastable materials[1,2] with interesting physical properties, for example metallic glasses, quasicrystals, and nanocrystals. Using thin-film techniques, extended compositional ranges of glass formation can be achieved, in addition to a convenient form for characterization of the materials and investigation of their physical properties.

Heavy-ion irradiation[3,4] of elemental multilayers has proved to be a useful method to synthesize metallic amorphous[5–18] and quasicrystalline[14–18] thin films. The collision cascades created by energetic incident ions give rise to atomic mixing and metastable phase formation. Structurally simple metastable crystalline phases and amorphous phases have frequently been observed[3] after ion-beam mixing at low and intermediate temperatures. Previous studies[3,8,11,12,19] of amorphization by ion-beam mixing have suggested that metallic systems with large negative enthalpies of mixing and no competing simple crystalline phases quite generally can be amorphized by heavy-ion irradiation. The binary phase diagrams of aluminum–3*d* transition metals (M) exhibit[20,21] a series of structurally complex compounds on the aluminum-rich side and these alloy systems have relatively large negative enthalpies of mixing.[22] This suggests that aluminum-rich Al-M alloys, which have not been possible to amorphize by rapid quenching[23,24] from the melt, might be good candidates for amorphization using heavy-ion irradiation. Ion-beam mixing of binary Al-3*d*-transition-metal alloys has previously been investigated only for relatively few compositions and temperatures (Refs. 3, 6, 9–11, and 14–18).

The electrical properties of amorphous metals have been intensively investigated during the past two decades, but so far no generally accepted understanding has emerged.[25–28] Among the main problems are (1) the fundamental difficulty of properly describing transport in disordered structures, (2) how to treat systems with strong scattering of the conduction electrons, and (3) a shortage of experimental investigations of amorphous systems with relatively simple and well-known electron structures. Transport properties of low-resistivity amorphous metals consisting of non-transition-metals are relatively well understood[25] and widely thought to be possible to describe in terms of the free-electron model and its extension, the Ziman-Faber model.[29] Transition-metal-based amorphous metals generally show high resistivities with small, often negative, temperature coefficients. Free-electron-based models, like the Mott *s-d* scattering model,[30,31] the Ziman-Faber model and its extensions,[32] were previously thought to apply to such strong-scattering systems, but the apparent success of these models has in recent years been regarded as somewhat fortuitous.[26–28] Although the basic physical mechanisms in these models still are believed to be very relevant, additional effects[28], such as weak localization, electron-electron interaction, *s-d* hybridization, skew scattering and side jump, and *d*-band conduction appear to be important to understand, for example, the temperature dependence of the electrical resistivity, magnetoresistance, and the Hall effect. The electrical transport properties of amorphous binary aluminum-3*d* metals are interesting from the point of view that they do not belong to any of the typical classes of amorphous metals, like binary transition-metal alloys, transition-metal-metalloid alloys, or non-transition-metal alloys. Liquid aluminum has been regarded as a free-electron-like metal and in amorphous aluminum-rich Al-M alloys, the impact of transition-metal alloying in such a metal can be systematically studied. In addition, the *d*-electron characteristics[33–36] of these alloy systems are relatively simple and known. To our knowledge, no studies of the electrical properties of amorphous Al-M with changing transition-

metal element have previously been reported.

We present studies of amorphization using ion-beam mixing and of the electrical resistivity in thin films of Al-Ti, Al-V, Al-Cr, Al-Mn, Al-Fe, Al-Co, and Al-Ni. The phase formation has been investigated for 500-keV Xe^+ irradiation as a function of temperature during the irradiation and transition-metal content. Amorphization, which previously only has been reported (Refs. 3,6,9–11, and 14–18) for a few of these binaries, is observed in all these alloy systems at low temperatures. The electrical resistivity has been investigated in the amorphous state as a function of varying $3d$-transition-metal element, and a maximum is observed, which can be correlated to the element, where the d-electron states coincide with the Fermi level.

II. EXPERIMENTAL

Thin elemental multilayers, with individual layer thickness not exceeding 60 Å, were e-beam evaporated in pressure better than 2×10^{-7}Pa, measured immediately before and after the evaporations. A typical film consisted of 20 layers having a total thickness of about 1000 Å. The films were evaporated directly on sapphire or on sapphire partly covered by a thin NaCl layer. Some of the substrates were covered with masks during the evaporation giving a suitable film geometry for four-probe resistance measurements.

Rutherford backscattering spectrometry (RBS) was used to check the homogeneity of the films and to determine their composition and thickness. The composition of the films could be determined within 1 at. %. In addition, the thicknesses were measured using a stylus-force apparatus. The thicknesses determined by these independent methods were found to be in reasonable agreement. For the calculation of the absolute magnitude of the electrical resistivity, the thickness values obtained by RBS, which appeared to show less scatter, were used. The error in the absolute values of the electrical resistivities, arising mainly from the uncertainty in the thickness determination, is estimated to be less than 15%.

Irradiation with 500-keV Xe^+ ions were performed in a vacuum better than 1×10^{-4}Pa, with doses of 3×10^{16} ions/cm^2 below room temperature and 2×10^{16} ions/cm^2 at room temperature to ensure complete mixing of the elemental layers. The current was kept below 0.2 μA/cm^2 in order to avoid sample heating during the irradiation.

After the irradiations, the parts of films having a thin NaCl layer between the film and substrate were floated off in deionized water. The films were subsequently analyzed using a 200-kV transmission electron microscope (TEM), Philips CM-20. The amorphous phase was identified from broad diffraction haloes and featureless micrographs.

III. RESULTS

In Figs. 1–5, the phase formation after 500-keV Xe^+ irradiation of multilayered films of $Al_{1-x}Ti_x$, $Al_{1-x}V_x$, $Al_{1-x}Cr_x$, $Al_{1-x}Fe_x$, and $Al_{1-x}Ni_x$ are shown as a function of composition and substrate temperature. In these

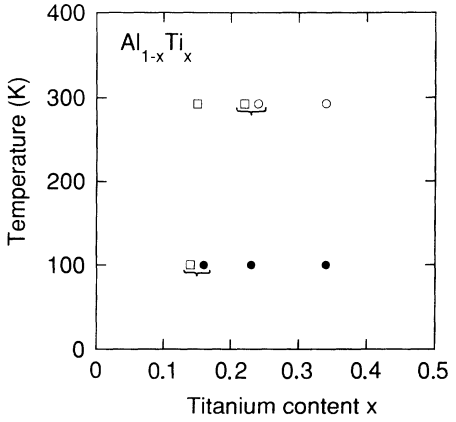

FIG. 1. The phase formation after 500-keV Xe^+ irradiation as a function of composition and substrate temperature for $Al_{1-x}Ti_x$. The symbols denote (●) amorphous phase, (□) fcc Al(Ti), and (○) hcp Al-Ti.

alloy systems, at 100 K complete amorphization could be achieved after irradiation of films with transition-metal contents between about 15 and 25 at. %, and in several cases the range of complete amorphization was found to be larger. The position of the first broad diffraction halo using TEM of the amorphized $Al_{1-x}M_x$ alloys was found to correspond to approximately $d=2.2$ Å showing only a weak or no dependence on composition for alloys containing more than 75 at. % aluminum. On the aluminum-rich side, the amorphous single-phase regions were limited by coexisting fcc Al(M). In all these alloy systems, the equilibrium solid solubility of transition metals in fcc Al is very limited.[20] The largest equilibrium solid solubility, being only 0.20 at. %, is found for vanadium. With ion-beam mixing and rapid solidification, solid solubilities extended beyond equilibrium can quite routinely be achieved.[3,23,24] The lattice constants of the fcc Al(M) phase was found to be reduced by typically up to 2% as compared to that of pure aluminum, suggesting M contents of several percents. However, no detailed analysis of the dissolved transition-metal content in fcc

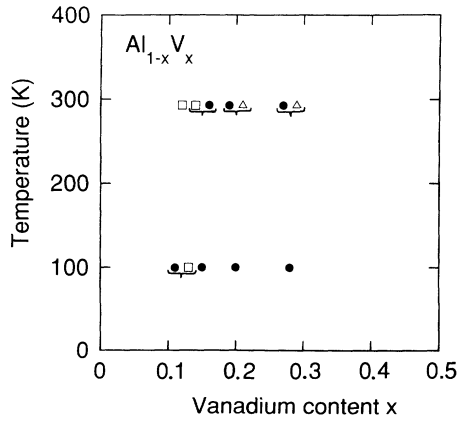

FIG. 2. Same as Fig. 1 for $Al_{1-x}V_x$. The symbols denote (●) amorphous phase, (□) fcc Al(V), and (△) bcc Al-V exhibiting superlattice reflections indicating CsCl-type ordering.

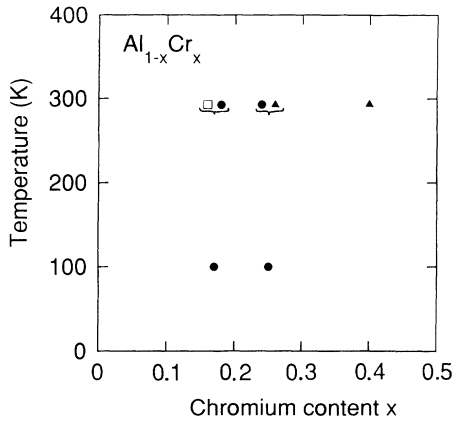

FIG. 3. Same as Fig. 1 for $Al_{1-x}Cr_x$. The symbols denote (●) amorphous phase, (□) fcc Al(Cr), and (▲) bcc Al-Cr.

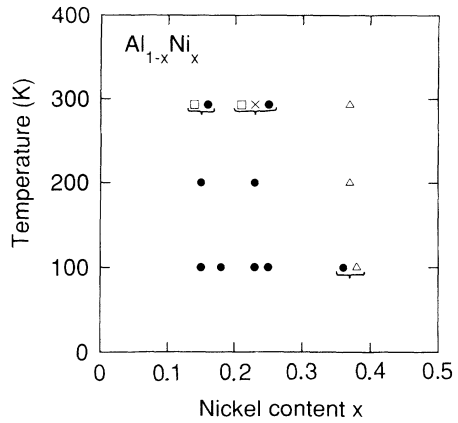

FIG. 5. Same as Fig. 1 for $Al_{1-x}Ni_x$. The symbols denote (●) amorphous phase, (□) fcc Al(Ni), (×) Al_3Ni_2 and (△) bcc Al-Ni exhibiting superlattice reflections indicating CsCl-type ordering.

Al has been performed due to the limited accuracy of lattice-constant measurements obtained from transmission electron diffraction.

On the transition-metal-rich side, see Figs. 1–5, structurally simple crystalline phases are found to appear in addition to the amorphous phases. For Al-Ti (Fig. 1), at room temperature, extended solid solutions of the elemental structures, fcc and hcp, are observed. The extended region of the hcp solid solution appear to be in accordance with the considerable equilibrium solubility of aluminum in hcp titanium.[20] For Al-Ti at low temperatures, amorphization is achieved instead for the same compositions. For Al-V, Al-Cr, Al-Fe, and Al-Ni (Figs. 2–5), the amorphous phase region is limited on the transition-metal-rich side by coexisting bcc solid solutions both at room temperature and at the lowest temperature. The equilibrium solid solubility of aluminum in bcc vanadium and bcc chromium is large. In both the equilibrium phase diagrams of Al-Fe and Al-Ni bcc phases having CsCl-type order with relatively wide phase fields are present. The bcc phases found after irradiation exhibit CsCl-type order for Al-V (see also Ref. 37) and Al-Ni, as evidenced by the appearance of superlattice reflections. No evidence for superlattice reflections could be observed for Al-Cr and Al-Fe, suggesting that the bcc lattice positions are randomly occupied after the irradiation. To summarize, we find that in no case could the crystalline equilibrium structures corresponding to a specific film composition be observed after ion-beam mixing. Instead, amorphous phases and extended hcp or bcc solid solutions, the latter showing CsCl ordering in some cases, are observed at room temperature and below.

In Fig. 6, the absolute magnitude of the electrical resistivities at room temperature are shown for binary amorphous $Al_{1-x}M_x$ thin films with M=Ti, V, Cr, Mn, Fe, Co, and Ni. The solid triangle at $x=0$ corresponds to liquid aluminum[38] at the melting temperature. For all alloys the resistivity is observed to increase with transition-metal content. For alloys having a electrical resistivities below 200 $\mu\Omega$ cm, the resistivity increase from the liquid state ($x=0$) appears to be approximately

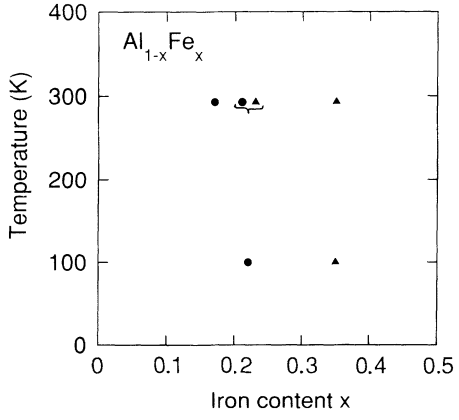

FIG. 4. Same as Fig. 1 for $Al_{1-x}Fe_x$. The symbols denote (●) amorphous phase, (□) fcc Al(Fe), and (▲) bcc Al-Fe.

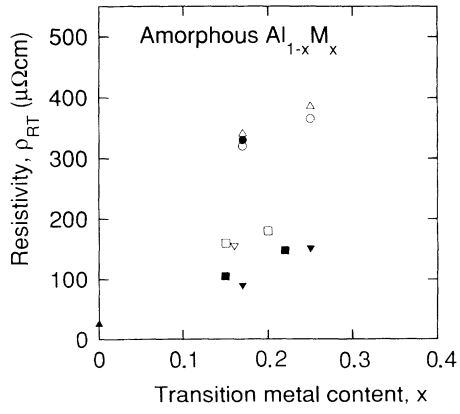

FIG. 6. The electrical resistivity of amorphous $Al_{1-x}M_x$ alloys measured at room temperature as a function of transition-metal content. The symbols denote (■) Ti, (□) V (Ref. 14), (○) Cr, (●) Mn (Ref. 15), (△) Fe, (▽) Co, and (▼) Ni. The symbol (▲) at $x=0$ corresponds to liquid Al at the melting temperature.

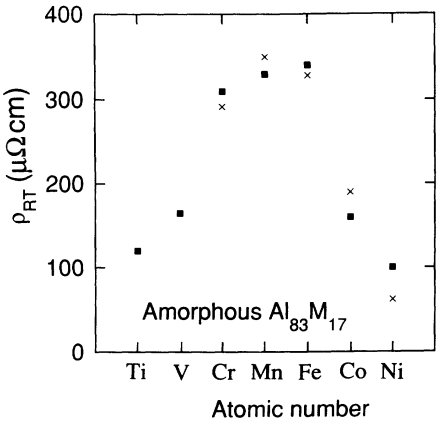

FIG. 7. The electrical resistivity of amorphous $Al_{83}M_{17}$ alloys as a function of changing transition metals (M) are shown as filled symbols. The crosses (×) correspond to the resisivity calculated according to the empirical expression in Eq. (2).

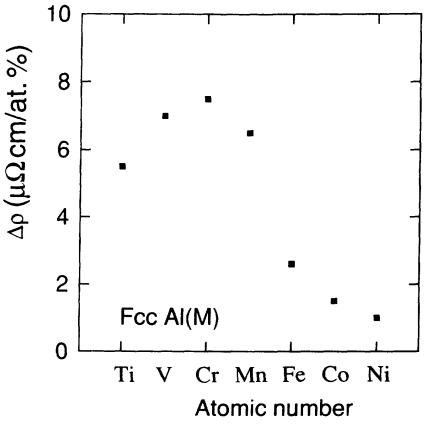

FIG. 8. The increase in residual resistivity in dilute fcc Al(M) alloys as a function of changing transition metals from Refs. 44–46. Note that here a maximum is observed for Cr, whereas for amorphous $Al_{83}TM_{17}$, in Fig. 7, a maximum is found for Fe.

TABLE I. Physcial data estimated for amorphous Al-M alloys.

M	Resistivity of a-$Al_{83}M_{17}$ ($\mu\Omega$ cm)	Δ[a] (eV)	(E_F-E_0)[b] (eV)	Enthalpy of Mixing[c] for $Al_{0.5}$-$M_{0.5}$ (kJ/mol)
Ti	120		neg.	−61
V	165		neg.	−40
Cr	310	1.53	−0.7	−30
Mn	330	0.72	0.0	−43
Fe	340	0.77	0.2	−32
Co	160	0.82	0.8	−43
Ni	100	0.61	1.7	−48

[a]Estimates taken from experimental XPS data (Ref. 33), except for Cr for which a calculated (Ref. 42) width was selected.
[b]From Ref. 33 with a shift of 0.7 eV (see text).
[c]Enthalpy of mixing of an ordered compound calculated from the semiempirical theory of Miedema (Ref. 22).

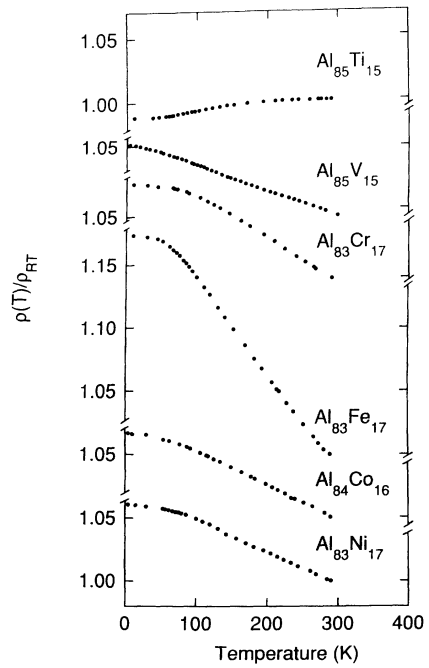

FIG. 9. The electrical resistivity normalized to room temperature for amorphous Al-M films.

proportional to the transition-metal content.

In Fig. 7 and in Table I, the resistivity data in Fig. 6, have been interpolated to the same composition of $Al_{83}M_{17}$ to illustrate the dependence on changing transition-metal element. A broad maximum of 340 $\mu\Omega$ cm is found around iron. For comparison, the increase in residual resistivity on transition-metal alloying of dilute fcc Al(M) is shown in Fig. 8. The behavior is quantitatively similar, but the maximum is observed to be shifted from Cr for the dilute crystalline state to Fe for the amorphous $Al_{83}M_{17}$.

In Fig. 9, the normalized resistivity is shown as a function of temperature. All the amorphous alloys, except $Al_{83}Ti_{17}$, are found to exhibit a negative temperature coefficient of resistivity. In Fig. 10, the negative tempera-

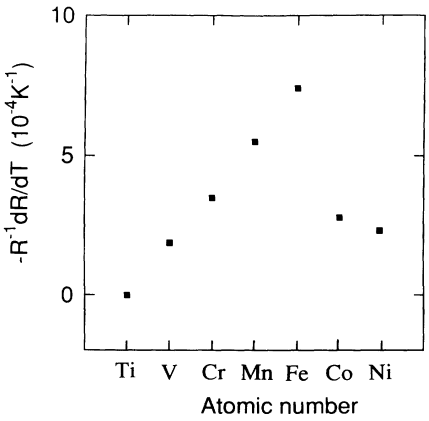

FIG. 10. The temperature coefficient of the electrical resistivity at room temperature for the same films as in Fig. 9.

ture coefficient of resistivity at room temperature is shown for the same alloys (data for Al-V and Al-Mn are from Refs. 14 and 15).

IV. DISCUSSION

During ion-beam mixing at low temperatures, where conventional radiation-enhanced diffusion is negligible, the atomic mixing and phase formation are believed[3] to occur mainly during the cooling-down of the collision cascade regions. The cooling rate of a cascade depends on, for example, the energy and masses of the ions and the target elements, the thermophysical properties of the solid, and the substrate temperature. Previous estimates[3,4] suggest that the time for the cooling down of typical heavy-ion collision cascade is much shorter than one nanosecond. This appears to be in agreement with the common observation[5–19] that structurally complex phases, presumably having low nucleation and growth rates, are not observed after ion-beam mixing at low temperatures.

Amorphization is thermodynamically possible during ion irradiation if the free energy of the amorphous phase is lower than that of the competing crystalline phases. This may occur, for example, if the free energy of the competing crystalline phases is enhanced due to radiation induced defects, or if nucleation and growth of the crystalline phases having a lower free energy than the amorphous phase are kinetically inhibited. As mentioned previously, the formation of structurally complex equilibrium compounds,[21] which are present quite generally in the binary aluminum-3*d* transition-metal phase diagrams for aluminum-rich compositions, is not observed here during heavy-ion irradiation at room temperature and below. Implantation of manganese in a single crystal of aluminum has shown[39] that complete amorphization occurs for Mn concentrations larger than 15 at. %. Approximately the same transition-metal contents appear to be sufficient to achieve amorphization with 500 keV Xe^+ irradiation of the $Al_{1-x}Ti_x$, $Al_{1-x}V_x$, $Al_{1-x}Cr_x$, $Al_{1-x}Fe_x$, and $Al_{1-x}Ni_x$ films investigated here.

As mentioned, in Al-V, Al-Cr, Al-Fe, and Al-Ni, the region of complete amorphization is limited on the transition-metal-rich side by the appearance of bcc phases. Evidence is found for order of the CsCl-type (the *B*2 structure) only for Al-V and Al-Ni. In a simple nearest-neighbor bond model of the bcc structure,[3] the enthalpy of mixing of the CsCl-type ordered structure is $1\frac{1}{2}$ times that of disordered bcc. In Table I, the enthalpies of mixing of the ordered compounds of $Al_{0.50}M_{0.50}$, estimated using the semi-empirical Miedema model[22] are shown. It is interesting to see that here the CsCl-type order is only observed after ion irradiation for Al-V and Al-Ni, which have the largest enthalpies of mixing of the presently investigated alloys and thus presumably the largest driving forces for forming ordered structures.

The electronic structure of dilute fcc Al(*M*) alloys consists of a wide *sp*-conduction band and a narrow localized *d* band.[33] In the Friedel-Anderson model,[40,41] the *d* band is described as a virtual bound state (VBS) having a characteristic width 2Δ and energy E_0. The total density of states $N(E_F)$ at the Fermi level with a contribution from the VBS $N_d(E_F)$ can be approximated by[40,41]

$$N(E_F)=N_{sp}(E_F)+N_d(E_F) \approx N_{sp}(E_F)+x\frac{10}{\pi}\frac{\Delta}{\Delta^2+(E_F-E_0)^2}\ , \quad (1)$$

where x is the concentration of 3*d*-transition metals. The *d*-electron contribution to the density of states at the Fermi level, and thus also its impact on electrical transport properties, depends sensitively on the energy difference (E_F-E_0) and width Δ of the VBS. Studies of x-ray photoelectron spectroscopy[33] (XPS) have confirmed the existence of a VBS in dilute Al(*M*) alloys. Furthermore, the relative energies of the VBS for various transition-metal elements in the dilute crystalline case have been determined and their widths have been estimated both experimentally[33] and theoretically.[42,43] These XPS investigations[33] indicate that (1) the energy of the 3*d*-electron states E_0, relative to the Fermi level, is systematically increasing with decreasing atomic number in the 3*d*-transition-metal series, (2) the 3*d*-electron states coincide with the Fermi-level approximately for chromium, and (3) the intensity of the 3*d*-states in XPS is found to be approximately proportional to the transition-metal content in Al(*M*). These observations appear to be in good agreement with earlier investigations of electrical transport properties in the dilute crystalline state.[36,44–46]

For the purpose of this study, the *d*-electron states in amorphous $Al_{83}M_{17}$ rather than in dilute fcc Al(*M*) are of interest. The relatively few existing XPS investigations of concentrated Al-*M* alloys[33–35] have demonstrated a slight increase in the width and shift in energy E_0 relative to E_F on alloying with up 50 at. % transition metals. The relative energy shift of E_0, obtained by comparing XPS data from the literature can be estimated to 0.6 eV for AlNi (Refs. 33 and 35) and 0.3 eV for Al_2Cu (Refs. 33 and 34). A comparison between XPS data[33] and calculations on Al_4Mn (Ref. 47) indicate an energy shift of 0.7 eV. Due to the lack of systematic information, we will assume that an energy shift of 0.7 eV is appropriate for all the aluminum-rich amorphous $Al_{1-x}M_x$ alloys in the present study (extrapolating the XPS data from dilute alloys). In Table I, the position of the VBS E_0 obtained by shifting the experimentally determined[33] values of the various dilute Al(*M*) alloys are shown. An increased width Δ due to alloying and structural disorder should be expected, but on the other hand it should be noted that the values for Δ derived using XPS already contains an additional broadening due to the technique itself.[33] Therefore, the values for the widths from Ref. 33 are shown in Table I without any corrections. These values must be regarded as relatively uncertain for amorphous $Al_{1-x}M_x$ alloys. Similar values for the width in the range of 0.5–1.0 eV have also been suggested from model calculations of a disordered Al_4Mn alloy.[47] It is of interest to note that the VBS model has been used successfully to describe the transport and magnetic properties of icosahedral Al-Mn alloys.[47–49]

We will now suggest an empirical expression to de-

scribe our resistivity data on amorphous $Al_{1-x}M_x$. Just like in the Mott *s-d* scattering model and the extended Ziman-Faber model, the resistivity increase on alloying is suggested to be proportional to the *d*-density of states multiplied by the width of the *d*-states.[50] In the case of aluminum-rich amorphous $Al_{1-x}M_x$, we assume that the 3*d*-states can be described as a VBS and the *d*-density of states can be approximated by Eq. (1). This leads to the following expression

$$\rho=(1900\ \mu\Omega\,\mathrm{cm})x\frac{\Delta^2}{\Delta^2+(E_F-E_0)^2}+\rho^{\mathrm{liq\ Al}}\ . \qquad (2)$$

A small term $\rho^{\mathrm{liq\ Al}}$ was added in order to obtain good agreement with the experimental results in Fig. 6 for small values of x. Except for this term, the expression in Eq. (2) is very close to expressions derived previously from the Mott *s-d* scattering model.[30,31,51] To obtain complete agreement with the latter expressions,[31,51] our empirically fitted constant of proportionality in Eq. (2), 19 $\mu\Omega$ cm/at. %, should be replaced by more complicated expressions containing E_0 and k_F. In Fig. 7, the calculated resistivities according to Eq. (2) are shown. The good correlation between calculated and experimental resistivity data suggests that our simplified VBS version of the Mott *s-d* model appear to describe the composition dependence of the electrical resistivity of amorphous $Al_{1-x}M_x$ alloys.

As mentioned previously, systematic studies of the resistivity in dilute fcc Al(*M*) have been performed[44–46] (see Fig. 8), and these results have been consistently explained by the Friedel-Anderson model of scattering from a virtual bound state of the transition-metal *d*-states.[36,52] A qualitatively resembling dependence of the resistivity in dilute fcc Al(*M*) (Refs. 44–46) and amorphous $Al_{83}M_{17}$ as a function of the transition-metal element is found. The maximum for the amorphous $Al_{83}M_{17}$ alloys (Fig. 7) is found to be shifted in the direction to heavier transition-metal elements compared to the maximum in dilute crystalline state of fcc Al(*M*) (Fig. 8), which is consistent with our previous assumption of a 0.7-eV shift of the *d*-states. The rate of increasing residual resistivity with increasing transition-metal content in the dilute crystalline state (7.5 $\mu\Omega$ cm/at. % for Cr) is considerably lower than the experimental ones of amorphous Al-*M* in Fig. 6. This could be due to an increased efficiency of the transition-metal scattering in the amorphous state and presumably also to a decreasing number of effective *sp*-conduction electrons in the amorphous state. The impact of *s-d* hybridization,[28,53–54] not taken into account in the extended Ziman-Faber model and the Mott *s-d* scattering model is likely to be important for a better understanding of this aspect of the transport properties.

On changing the transition-metal element, the negative temperature coefficient of resistivity (Fig. 10), as well as the absolute magnitude of the electrical resistivity (Fig. 6) are found to increase monotonically from Ti to Fe and to decrease monotonically from Fe to Ni. This behavior appears to be in general agreement with Mooij's[55] empirical correlation. In order to understand the temperature dependence of the electrical resistivity and other transport properties like the Hall effect, the simplified approach used here is not believed to be sufficient even for a qualitative understanding. For example, within the Mott *s-d* scattering model the temperature dependence of amorphous metals is predicted to be much smaller than that observed experimentally.[28] The Hall effect has previously been observed to exhibit a sign change on changing composition in amorphous $Al_{1-x}V_x$.[14] The origin of the temperature dependence of high-resistivity amorphous alloys appears not to be understood, except at low temperatures where weak localization and electron-electron interaction appear to be dominating.[28]

ACKNOWLEDGMENTS

N. Karpe would like to acknowledge generous support from Naturvetenskapliga Forskningsrådet and Nordiska Ministerrådet for his stay at the University of Aarhus.

*Present address: Department of Solid State Physics, Royal Institute of Technology, S-100 44, Stockholm, Sweden.

[1]W. L. Johnson, Prog. Mater. Sci. **30**, 81 (1986).
[2]K. Samwer, Phys. Rep. **161**, 1 (1988).
[3]M. Nastasi and J. W. Mayer, Mater. Sci. Rep. **6**, 1 (1991).
[4]G. S. Was, Prog. Surf. Sci. **32**, 211 (1990).
[5]B. Y. Tsaur, S. S. Lau, L. S. Hung, and J. W. Mayer, Nucl. Instrum. Methods **182/183**, 67 (1983).
[6]L. S. Hung, M. Nastasi, J. Gyulai, and J. W. Mayer, Appl. Phys. Lett. **42**, 672 (1983).
[7]M. Nastasi, L. S. Hung, and J. W. Mayer, Appl. Phys. Lett. **43**, 831 (1983).
[8]M. Nastasi, D. Lilienfield, H. H. Johnson, and J. W. Mayer, J. Appl. Phys. **59**, 4011 (1986).
[9]Q. Z. Hong, D. A. Lilienfield, and J. W. Mayer, J. Appl. Phys. **64**, 4478 (1988).
[10]C. Jaouen, J. P. Rivière, A. Bellara, and J. Delafond, Nucl. Instrum. Methods B **7/8**, 591 (1985).
[11]C. Jaouen, J. P. Rivière, and J. Delafond, Nucl. Instrum. Methods B **19/20**, 549 (1987).
[12]B. Brennier, T. Capra, P. Thevenard, A. Perez, M. Treilleux, J. Rivory, J. Dupuy, and G. Guiraud, Phys. Rev. B **41**, 11 784 (1990); K. Pampus, K. Dyrbye, B. Torp, and R. Bormann, J. Mater. Res. **4**, 1385 (1989); J. Bøttiger, K. Dyrbye, K. Pampus, and R. Poulsen, Philos. Mag. A **59**, 569 (1989).
[13]L. U. Aaen Andersen, J. Bøttiger, and K. Dyrbye, Nucl. Instrum. Methods B **51**, 125 (1990).
[14]N. Karpe, L. U. Aaen Andersen, K. Dyrbye, J. Bøttiger, and K. V. Rao, Phys. Rev. B **39**, 9874 (1989).
[15]N. Karpe, K. V. Rao, J. Bøttiger, and B. Torp, Europhys. Lett. **4**, 323 (1987).
[16]D. M. Follstaedt and J. A. Knapp, J. Appl. Phys. **59**, 1756 (1986).
[17]D. A. Lilienfeld, M. Nastasi, H. H. Johnson, D. G. Ast, and J. W. Mayer, Phys. Rev. B **34**, 2985 (1986).
[18]K. Hohmuth, V. Heera, and B. Rauschenbach, Nucl. Instrum. Methods. B **39**, (1989).
[19]K. Kyllesbech Larsen, N. Karpe, J. Bøttiger, and R. Bor-

mann, J. Mater. Res. **7**, 861 (1992).
[20]T. M. Massalski, *Binary Phase Diagrams* (American Society for Metals, Metals Park, OH 1986).
[21]C. L. Henley, J. Non-Cryst. Solids **75**, 91 (1986).
[22]F. R. de Boer, R. Boom, W. C. M. Mattens, A. R. Miedema, and A. K. Nissen, *Cohesion in Metals–Transition-Metal Alloys* (North-Holland, Amsterdam, 1988).
[23]R. J. Schaefer, Scr. Metall. **20**, 1187 (1986).
[24]D. Shechtman, R. J. Schaefer, and F. S. Biancaniello, Metall. Trans. **15A**, 1987 (1984).
[25]U. Mizutani, Prog. Mater. Sci. **28**, 97 (1983).
[26]D. G. Naugle, J. Phys. Chem. Solids **45**, 367 (1984).
[27]J. S. Dugdale, Contemp. Phys. **28**, 547 (1987).
[28]M. A. Howson and B. L. Gallagher, Phys. Rep. **170**, 265 (1988).
[29]T. E. Faber and J. Ziman, Philos. Mag. **11**, 153 (1965).
[30]N. F. Mott, Philos. Mag. **26**, 1249 (1972).
[31]D. Brown, S. Fairbairn, and G. J. Morgan, Phys. Status Solidi B **93**, 617 (1979).
[32]R. Evans, D. A. Greenwood, and P. Lloyd, Phys. Lett. A **35**, 57 (1971).
[33]P. Steiner, H. Höchst, W. Steffen, and S. Hüfner, Z. Phys. B **38**, 191 (1980).
[34]J. C. Fuggle, L. M. Watson, D. J. Fabian, and P. R. Norris, Solid State Commun. **13**, 507 (1973).
[35]S. P. Kowalczyk, G. Apai, G. Kaindl, F. R. McFeely, L. Ley, and D. A. Shirley, Solid State Commun. **25**, 847 (1978).
[36]J. S. Dugdale, *The Electrical Properties of Metals and Alloys* (Arnold, London, 1977).
[37]The metastable bcc phase called the "*x*-phase" in Ref. 14 can be identified with a CsCl-type ordered bcc structure. Phases exhibiting the CsCl-type structre (*B2*) are present in the equilibrium phase diagrams of Al-Fe , Al-Co, and Al-Ni, but not in Al-V. The lattice constant corresponding to the metastable *B2* phase of Al-V observed in Ref. 14 is 2.07 Å.
[38]See G. Busch and H.-J. Günterrodt, in *Solid State Physics,* edited by H. Ehrenreich, F. Seitz, and D. Turnbull (Academic, New York, 1974) Vol. 29, pp. 235.
[39]A. Seidel, S. Massing, B. Strehlau, and G. Linker, Phys. Rev. B **38**, 2273 (1988).
[40]J. Friedel, Can. J. Phys. **34**, 1190 (1956); J. Phys. Rad. **19**, 573 (1958); Nuovo Cimento, VII Suppl., 287 (1958).
[41]P. W. Anderson, Phys. Rev. **124**, 41 (1961).
[42]L. Dagens, Phys. Status Solidi B **93**, 279 (1979).
[43]E. Mrosan and G. Lehmann, Phys. Status Solidi B **87**, K21 (1978).
[44]R. Aoki and T. Ohtsuka, J. Phys. Soc. Jpn. **23**, 955 (1967).
[45]R. Aoki and T. Ohtsuka, J. Phys. Soc. Jpn. **26**, 651 (1969).
[46]C. R. Vassel, J. Phys. Chem. Solids **7**, 90 (1958).
[47]D. Pavuna, C. Berger, F. Cyrot-Lackmann, P. Germi, and A. Pasturel, Solid State Commun. **59**, 11 (1986).
[48]C. Berger, J. C. Lasjaunias, J. L. Tholence, D. Pavuna, and P. Germi, Phys. Rev. B **37**, 6525 (1988).
[49]C. Berger, L. C. Lasjaunias, and C. Paulsen, Solid State Commun. **65**, 441 (1988).
[50]B. L. Gallagher and D. Greig, J. Phys. F **12**, 1721 (1982).
[51]D. Nguyen-Manh, D. Mayou, G. J. Morgan, and A. Pasturel, J. Phys. F **17**, 999 (1987).
[52]G. Grüner and A. Zawadowski, Rep. Prog. Phys. **37**, 1497 (1974).
[53]D. Mayou, D. Nguyen-Manh, A. Pasturel, and F. Cyrot-Lackmann, Phys. Rev. B **33**, 3384 (1986).
[54]G. F. Weir, M. A. Howson, B. L. Gallagher, and G. J. Morgan, Philos. Mag. **47**, 163 (1983).
[55]J. H. Mooij, Phys. Status Solidi A **17**, 321 (1973).